Glycolytic Pfkp acts as a Lin41 protein kinase to promote endodermal differentiation of embryonic stem cells

Leixi Cao[1,†], Ruijie Wang[1,†], Guangzhi Liu[1] (iD), Yuwei Zhang[1], Rick Francis Thorne[1,2] (iD), Xu Dong Zhang[1,3] (iD), Jinming Li[1] (iD), Yang Xia[4], Lili Guo[4] (iD), Fengmin Shao[1,*], Hao Gu[4,**] (iD) & Mian Wu[1,5,6,***] (iD)

Abstract

Unveiling the principles governing embryonic stem cell (ESC) differentiation into specific lineages is critical for understanding embryonic development and for stem cell applications in regenerative medicine. Here, we establish an intersection between LIF-Stat3 signaling that is essential for maintaining murine (m) ESCs pluripotency, and the glycolytic enzyme, the platelet isoform of phosphofructokinase (Pfkp). In the pluripotent state, Stat3 transcriptionally suppresses Pfkp in mESCs while manipulating the cells to lift this repression results in differentiation towards the ectodermal lineage. Pfkp exhibits substrate specificity changes to act as a protein kinase, catalyzing serine phosphorylation of the developmental regulator Lin41. Such phosphorylation stabilizes Lin41 by impeding its autoubiquitination and proteasomal degradation, permitting Lin41-mediated binding and destabilization of mRNAs encoding ectodermal specification markers to favor the expression of endodermal specification genes. This provides new insights into the wiring of pluripotency-differentiation circuitry where Pfkp plays a role in germ layer specification during mESC differentiation.

Introduction

Embryonic stem cells (ESCs) derived from the blastocyst inner cell mass are able to differentiate into all somatic cell types (Evans & Kaufman, 1981; Martin, 1981). Based on these pluripotent properties, ESCs have been promoted for potential use in regenerative medicine and cell-based therapies. In mouse ESCs (mESCs), pluripotency is orchestrated by a select group of transcription factors including Oct4, Sox2, Klf4, c-Myc, Nanog, and Stat3, which together direct an intricate regulatory network that maintains ESC identity (Nichols et al, 1998; Niwa et al, 1998; Chambers et al, 2003; Mitsui et al, 2003; Boyer et al, 2005; Hall et al, 2009). Indeed, the activities of these core pluripotency factors have been harnessed for reprogramming somatic cells using the induced pluripotent stem cell (iPSC) technology (Takahashi & Yamanaka, 2006). Additionally, certain soluble substances including the IL-6 family cytokine member leukemia inhibitory factor (LIF) are also essential for maintaining pluripotency in vitro (Smith et al, 1988; Williams et al, 1988). LIF acts by binding to the LIF receptor (LIFR) on the surface of mESCs, which forms part of a larger complex involving gp130 together with cytoplasmic Jak family tyrosine kinases. Subsequent Tyr 705 phosphorylation and activation of Stat3 induces its nuclear translocation (Fu et al, 1990, 1992; Schindler et al, 1992; Darnell Jr et al, 1994), which in turn drives the transactivation of core pluripotency genes including Oct4 and Nanog (Ying et al, 2003; Do et al, 2013). Therefore, LIF-Stat3 signaling plays an essential role in pluripotency maintenance and lineage specification.

Intriguingly, the metabolic signature of embryonic stem cells is similar to that of cancer cells, showing a strongly glycolytic phenotype (Vander Heiden et al, 2009). Notably, when ESCs undergo differentiation, their metabolic profile switches towards reliance on

1 Translational Research Institute, Henan Provincial People's Hospital, Academy of Medical Science, Zhengzhou University, Zhengzhou, China
2 School of Biomedical Sciences & Pharmacy, University of Newcastle, Newcastle, NSW, Australia
3 School of Environmental & Life Sciences, University of Newcastle, Newcastle, NSW, Australia
4 Department of Immunology, School of Basic Medical Sciences, Anhui Medical University, Hefei, China
5 School of Clinical Medicine, Henan University, Zhengzhou, China
6 CAS Centre for Excellence in Molecular Cell Science, the First Affiliated Hospital of University of Science and Technology of China, Hefei, China
  *Corresponding author. Tel: +86 0371 65581626; E-mail: fengminshao@126.com
  **Corresponding author. Tel: +86 0551 65161139; E-mail: guhao@ahmu.edu.cn
  ***Corresponding author. Tel: +86 0371 87160233; E-mail: wumian@ustc.edu.cn
  †These authors contributed equally to this work

oxidative phosphorylation (Gu *et al*, 2016; Cliff *et al*, 2017). Glycolysis rapidly liberates the high-energy compounds ATP and NADH from glucose, but nonetheless, the resultant pyruvate together with other glycolytic intermediates are key substrates for a variety of relevant pathways. For instance, one of the fates of pyruvate-derived acetyl-CoA involves regulating histone acetylation, which is indispensable for the maintenance of the epigenetic identity of human (h) ESC (Moussaieff *et al*, 2015). Furthermore, the modulation of glycolysis can directly impact pluripotency maintenance in human and mouse ESCs, e.g., reductions in glycolysis enhance neural differentiation in human ESCs (Gu *et al*, 2016). Notably, hexokinase 2 (HK2) and pyruvate kinase M2 (PKM2), which are rate-limiting glycolytic enzymes, have been shown to impair lineage specification in ESCs in the absence of LIF (Kim *et al*, 2015). On the other hand, the expression of glycolytic enzymes is also directly regulated by the core pluripotency factors; Oct4 dictates the rate of glycolytic flux in mESCs via the transcription of *HK2* and *PKM2* (Kim *et al*, 2015) while SOX2, OCT4, and NANOG promote glucose uptake and glycolysis in hESCs by inducing GLUT1 expression (Yu *et al*, 2019). However, whether crosstalk exists between LIF-Stat3 signaling and glycolysis in the maintenance of ESC pluripotency remains an open question.

Of interest to this report is Lin41, a member of the Trim-NHL protein family, which functions as a conserved developmental regulator in *Caenorhabditis elegans* and vertebrates as well as serving as a reprogramming factor (Reinhart *et al*, 2000; Chen *et al*, 2012; Schulman *et al*, 2014; Worringer *et al*, 2014). Lin41 possesses both E3 ubiquitin ligase activity and RNA-binding capabilities by virtue of its N-terminal tripartite motif (Trim) domain and C-terminal NHL (NCL-1, HT2A2, and LIN-41) repeat domains, respectively (Kwon *et al*, 2013). Both the ubiquitination and RNA-binding activities have been associated with pluripotency regulation. For example, the SHC binding and spindle associated 1 (SHCBP1) protein were identified as a Lin41 ubiquitination substrate and their interaction shown to underly the defects in neurogenesis observed in Lin41-deficient ES cells (Chen *et al*, 2012). Moreover, Lin41-dependent ubiquitination of p53 was also reported to be crucial for cell fate specification during early brain development (Nguyen *et al*, 2017). Alternatively, Lin41 was shown to suppress the translation of the differentiation-promoting gene *EGR1* to enhance somatic cell reprogramming (Worringer *et al*, 2014). Lin41 also enjoys a special relationship with the let-7 microRNA (miR) family, which controls stem cell differentiation by suppressing the expression of pluripotency genes (Rybak *et al*, 2008). On the one hand, Lin41 is negatively regulated by let-7 miRs at the mRNA level (Reinhart *et al*, 2000) while Lin41 also inhibits the translation of Ago2 mRNA, which, in turn, influences the RNA-induced silencing complex (RISC) and maturation of let-7 miRs (Liu *et al*, 2021). Nonetheless, there are still open questions about the precise relationship between miR-mediated repression and the functions of Lin41 (Connacher & Goldstrohm, 2021).

This study was initiated to investigate the potential contribution of LIF-Stat3 signaling in glycolysis in mESCs. We discovered that the platelet isoform of phosphofructokinase (Pfkp), the rate-limiting enzyme of glycolysis, was an important target of Stat3 transcriptional repression in mESCs. Pfkp was shown to modulate germ layer differentiation via catalyzing protein phosphorylation of Lin41, resulting in its stabilization and ensuing downstream effects on the degradation of ectodermal specification mRNAs. Uncovering this mechanism provides deeper insights into the regulation of pluripotency maintenance and lineage specification in ESCs with implications towards clinical applications.

Results

Pfkp affects stemness in murine ESCs

To establish whether broad correlates existed between LIF-Stat3 signaling, glycolysis, and pluripotency, we surveyed the expression of all rate-limiting glycolytic enzymes after manipulating Stat3 in mESCs using shRNA. Analysis by Western blotting of the different isoforms of hexokinase (Hk), phosphofructokinase (Pfk), and pyruvate kinase (Pk) showed there were significant increases in Pfkp levels after the knockdown of Stat3 (Fig 1A). In parallel, we conversely investigated the impact of knockdown of each of the rate-limiting glycolytic enzymes on the levels of the core pluripotency factors, namely c-Myc, Oct4, Nanog, Klf4, and Sox2. We observed that the levels of all pluripotency markers in mESCs declined when either Hk2 or Pfkl were silenced (Fig 1B and C, and Appendix Fig S1A and B), whereas knockdown of Hk1, Hk3, Pfkm, Pkm2, or Pklr had little impact on their levels (Fig 1D–H and Appendix Fig S1C–G). Surprisingly, knockdown Pfkp strongly enhanced the expression of all pluripotency markers, especially *Sox2* (Fig 1I and Appendix Fig S1H), suggesting Pfkp is a potential transcriptional target under repression by Stat3.

To next discern the contribution of the different Pfks to glycolytic flux in mESCs, we individually knocked down Pfkp, Pfkl, and Pfkm and measured changes in the extracellular acidification rate (ECAR) and levels of acetyl-CoA, respectively. Instructively, only Pfkl silencing led to decreased ECAR and acetyl-CoA production (Appendix Fig S1I and J). Moreover, quantitative comparisons of the protein levels of each of the three Pfk isoforms showed that Pfkl accounts for nearly 70% of total Pfk enzyme content followed by Pfkp with ~29% (Appendix Fig S1K). Thus, Pfkl is the major Pfk isoform promoting glycolysis in mESCs. However, while Pfkp is also expressed at comparatively high levels, it makes negligible contributions to glycolytic flux. Rather, the effects of Pfkp knockdown suggested an alternative role to balance pluripotency versus differentiation.

Pfkp is transcriptionally repressed by Stat3 in mESCs

Based on the preceding findings, we investigated the relationship between Stat3 and Pfkp in further detail. Indeed, we observed both mRNA and protein levels of Pfkp were upregulated in mESCs after Stat3 silencing (Fig 2A and B) while conversely their levels decreased when exogenous Stat3 was introduced (Fig 2C). Additionally, knockdown of Stat3 was shown to increase the levels of Pfkp pre-mRNA (Fig 2D), suggesting that Pfkp was being regulated at the transcriptional level. We next analyzed the promoter region of the *Pfkp* gene using a bioinformatics approach, with interrogation using the JASPAR database (https://jaspar.genereg.net/) uncovering three potential consensus Stat3 binding sites (Fig 2E). Of these, the two most proximal binding motifs located at −150 to −159 and −1,005 to −1,014 from the transcriptional start site were confirmed to be associated with Stat3 in ChIP assays (Fig 2F). Lastly, in the context
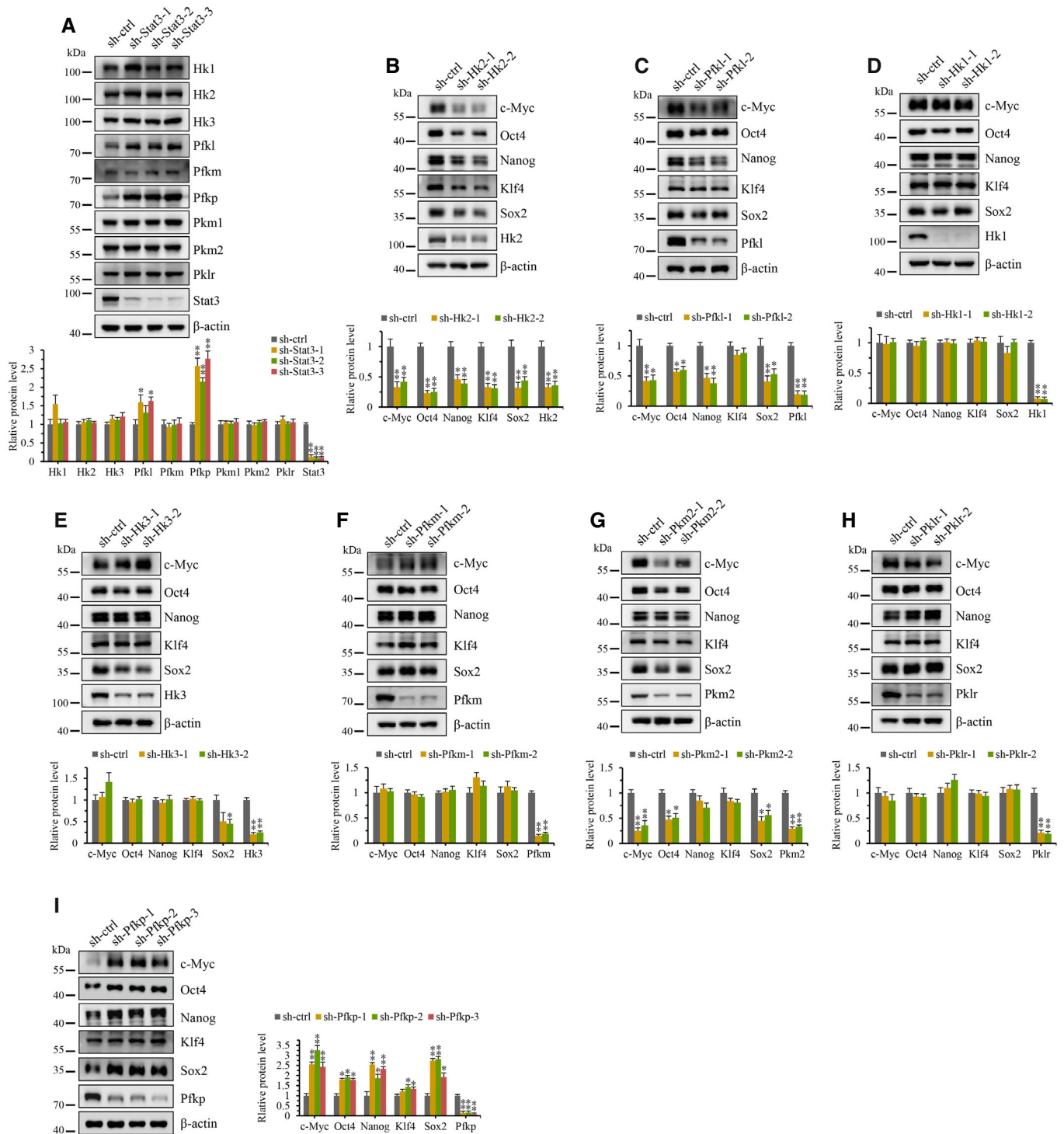
Figure 1. Stat3-dependent regulation of glycolytic enzyme expression in murine ESCs.

A   Expression of all rate-limiting glycolytic isoenzymes in R1 cells after the knockdown of Stat3 using three independent shRNAs compared with an empty vector control shRNA (sh-ctrl), as measured by Western blot. β-actin was employed as a loading control throughout.

B–I   Expression of the pluripotency genes c-Myc, Oct-4, Nanog, Klf4, and Sox-2 in R1 cells after the knockdown of Hk2 (B), Pfkl (C), Hk1 (D), Hk3 (E), Pfkm (F), Pkm2 (G), Pklr (H), and Pfkp (I) glycolytic enzymes using two or three independent shRNAs, as measured by Western blot.

Data information: The data were repeated three times and shown as the mean ± SD of three independent experiments. One asterisk and two asterisks indicate $P < 0.05$ and $P < 0.01$, respectively.

of luciferase reporter assays using the Pfkp promoter, ectopic expression of Flag-Stat3 resulted in transcriptional repression, with analyses of Stat3 binding motif mutants showed that the more proximal site (-150 to -159) was primarily responsible for the activity of Stat3 in these assays (Fig 2G). Together, these data establish that Stat3 acts to repress the expression of Pfkp in mESCs.

Pfkp modulates mESC differentiation

From the preceding results, silencing Pfkp increased the levels of pluripotency markers, implying Pfkp expression favors driving mESCs towards differentiation. To test this notion, we overexpressed Pfkp in mESCs and showed this not only downregulated the
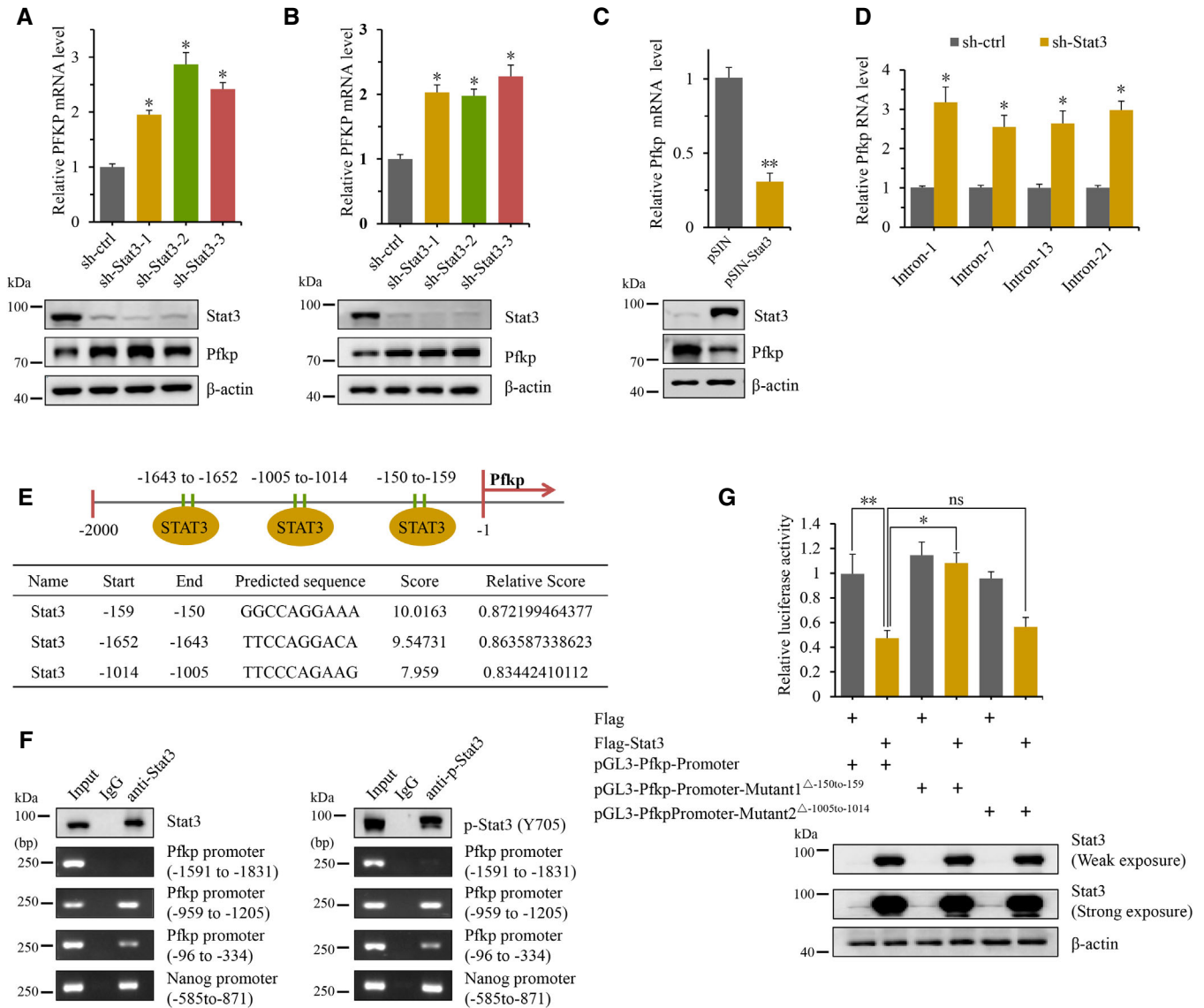
Figure 2. *Pfkp* is transcriptionally repressed by *Stat3* in murine ESCs.

A–C Expression of Pfkp mRNA levels (top panels) and Stat3 and Pfkp protein expression (bottom panels) after the knockdown of Stat3 using three independent shRNAs in either R1 cells (A) or E14 cells (B) or after overexpression of Stat3 in R1 cells (C), as measured by qPCR and Western blot, respectively. β-actin was employed as a loading control throughout.

D The levels of Pfkp pre-mRNA compared in sh-ctrl versus sh-Stat3 knockdown R1 cells, as measured by qPCR against the indicated Pfkp introns.

E, F Schematic showing the location of three Stat3 binding motifs in the *Pfkp* gene (E) with binding to Stat3 in R1 cells measured using ChIP assays against Stat3, p-Stat3 (Y705), or isotype-matched immunoglobulin G (IgG) (F), as measured by PCR, and images were representative of three independent experiments. Nanog promoter is shown as a positive control.

G Transcriptional activity of the indicated pGL3-based *Pfkp* promoter or mutant constructs expressed in HEK293T cells with or without overexpression of Stat3, as measured by luciferase reporter assay (top panel). Western blotting was used to verify Stat3 expression (bottom panel).

Data information: The data were repeated three times and shown as the mean ± SD of three independent experiments. One asterisk and two asterisks indicate $P < 0.05$ and $P < 0.01$, respectively.

levels of the core pluripotency markers (Fig 3A) but also resulted in morphological changes in mESCs that appeared consistent with differentiation (Fig 3B). Moreover, Pfkp overexpression also inhibited the levels of pluripotency markers in a Stat3-independent 2i culture medium (Appendix Fig S2A). Further analyses employing *in vitro* differentiation assays revealed that Pfkp expression was upregulated during both embryoid body formation and after LIF withdrawal from the culture medium (Fig 3C and D), suggesting that Pfkp acts to induce germ layer differentiation. After Pfkp was knocked down, the levels of core pluripotency markers were rescued in Stat3 silencing or LIF withdrawal ESCs, suggesting Pfkp is a fundamental mechanism by which Stat3 maintains pluripotency (Appendix Fig S2B and C).

Following this finding, we undertook a comparative transcriptomic analysis between control and Pfkp-knockdown differentiated ESC cultures to examine the expression of different lineage markers. Notably, many biological processes related to development and differentiation are listed among the top 20 Gene Ontology terms (Fig 3E). Further analysis revealed elevated levels of numerous ectodermal specification genes after Pfkp knockdown while conversely the expressions of endodermal and mesodermal specification genes were diminished (Fig 3F). As verification, selected ectodermal and endodermal genes were analyzed by qPCR and Western blotting, respectively, showing consistent increases in ectodermal markers and decreases in endodermal markers (Fig 3G–J). Moreover, mESC cultures directed towards endodermal differentiation derived smaller populations of Sox17 and Foxa2-positive cells when Pfkp was silenced (Fig 3K–N), and stronger expressions of endodermal markers were detected after Pfkp was overexpressed (Appendix Fig S2D and E). Furthermore, increased numbers of β-III Tubulin and neurofilament-L-positive cells were generated in Pfkp-knockdown mESCs using a neuronal differentiation protocol (Fig 3O–R). Together, these results indicated that Pfkp inhibits ectodermal differentiation and promotes endodermal differentiation of mESCs.

Pfkp binds to Lin41 and maintains its stability

We hypothesized that uncovering interactions between Pfkp and other proteins could help resolve the mechanism whereby Pfkp regulates germ layer differentiation. Towards this, Pfkp was immunoprecipitated from mESCs and mass spectrometry analysis used to identify a number of potential Pfkp-interacting proteins (Fig 4A). Besides Pfkp forming apparent heterodimers with Pfkl and/or Pfkm, we confirmed interactions with a number of candidate proteins including Lin41, Usp10, Catenin alpha-1, and Thoc4 (Fig 4B). Intriguingly, we observed that the expression of Lin41 was inhibited when Pfkp was knocked down (Fig 4C), so we kept our focus on the interaction between Pfkp and Lin41.

We next undertook domain mapping experiments to define the regions in the Pfkp and Lin41 proteins responsible for their interaction. The domain organization of the Lin41 protein consists of a RING domain, two B-box domains, two coiled-coil domains, one filamin domain, and six NHL repeats, while Pfkp can be divided into catalytic and regulatory domains (Fig 4D). We found that Lin41 lost the capability to bind with Pfkp only when both N- and C-terminal regions were deleted, suggesting that the RING domain, B-box domain and NHL repeats of Lin41 are responsible for Pfkp binding

(Fig 4E). Conversely, assays conducted with the catalytic and regulatory fragments of Pfkp show either domain could associate with Lin41 (Fig 4F). Further assessment of the binding capabilities of the individual N- and C-terminal Lin41 fragments showed both bound to the catalytic and regulatory domains of Pfkp, although the strength of interaction between the Pfkp catalytic domain and the NHL-repeat containing Lin41 C-terminal fragment was substantially weaker (Fig 4G). Thus, the interaction between Pfkp and Lin41 is direct and involves multifaceted interfaces between each molecule.

After defining the mode of interaction between Pfkp and Lin41, we returned to consider how Lin41 levels were regulated by Pfkp. Notably, while knockdown of Pfkp in mESCs lowered Lin41 protein levels, we found no changes in Lin41 mRNA levels (Fig 4H). Notably, silencing of Lin41 expression did not affect Pfkp mRNA or protein expression (Fig 4I), suggesting no feedback mechanism operated between Lin41 and Pfkp. Instructively, the decreases in Lin41 expression in mESCs after Pfkp knockdown could be rescued by treatment with proteasomal inhibitors (Fig 4J and K), whereas Pfkp overexpression was shown to enhance Lin41 protein stability (Fig 4L). Therefore, Pfkp functions to protect Lin41 from degradation, although the mechanism involved required further clarification.

Pfkp-catalyzed phosphorylation of Lin41 impairs its autoubiquitination activity

Previous studies of the Trim family have revealed the importance of posttranslational modification by phosphorylation in dictating activation and protein stability, for example, TRIM24 phosphorylation via ATM induces its autodegradation (Jain *et al*, 2014). Pfkp catalyzes the phosphorylation of fructose 6-phosphate in the glycolytic cascade, although we speculated its kinase activity could potentially extend to a noncarbohydrate substrate such as Lin41. Phosphorylation modifications of Lin41 have not been presently described, but a survey of total phosphorylation levels by Western blotting revealed strong signals for serine phosphorylation (Fig 5A). Furthermore, we found that ectopic expression of Pfkp greatly enhanced Lin41 phosphorylation, whereas Pfkp knockdown reduced these levels (Fig 5B). Decisive evidence was then provided using *in vitro* kinase assays where Pfkp was shown to catalyze the phosphorylation of Lin41 (Fig 5C). Gly33, Arg96, Cys97, Gly126, Asp127, Gly128, and Ser129 were demonstrated to be essential for ATP binding and Pfkp enzyme activity (https://www.uniprot.org). When Gly33 rather than other residues was mutated, both the sugar and protein kinase activities of Pfkp were abolished, suggesting Gly33 is indispensable for Pfkp activity and substrates share the same ATP binding site at Pfkp (Appendix Fig S3A–C). Moreover, an increasing amount of fructose-6-phosphate (F6P) inhibited the phosphorylation of Lin41 by Pfkp, and the generation of fructose-1,6-biphosphate was also suppressed after Lin41 protein was added, suggesting Lin41 and F6P competitively interact with Pfkp (Appendix Fig S3D and E). Additionally, *in vitro* analyses comparing Pfkp activity against its protein and sugar substrates indicated higher catalytic activity against Pfkp at lower substrate concentrations, peaking at ~1 μM, whereas the F-6-P substrate curve continued to increase (Appendix Fig S3F).

In order to better investigate the relationship between Pfkp-catalyzed Lin41 phosphorylation and protein stability, we used mass spectrometry analysis to identify phosphate-modified residues in
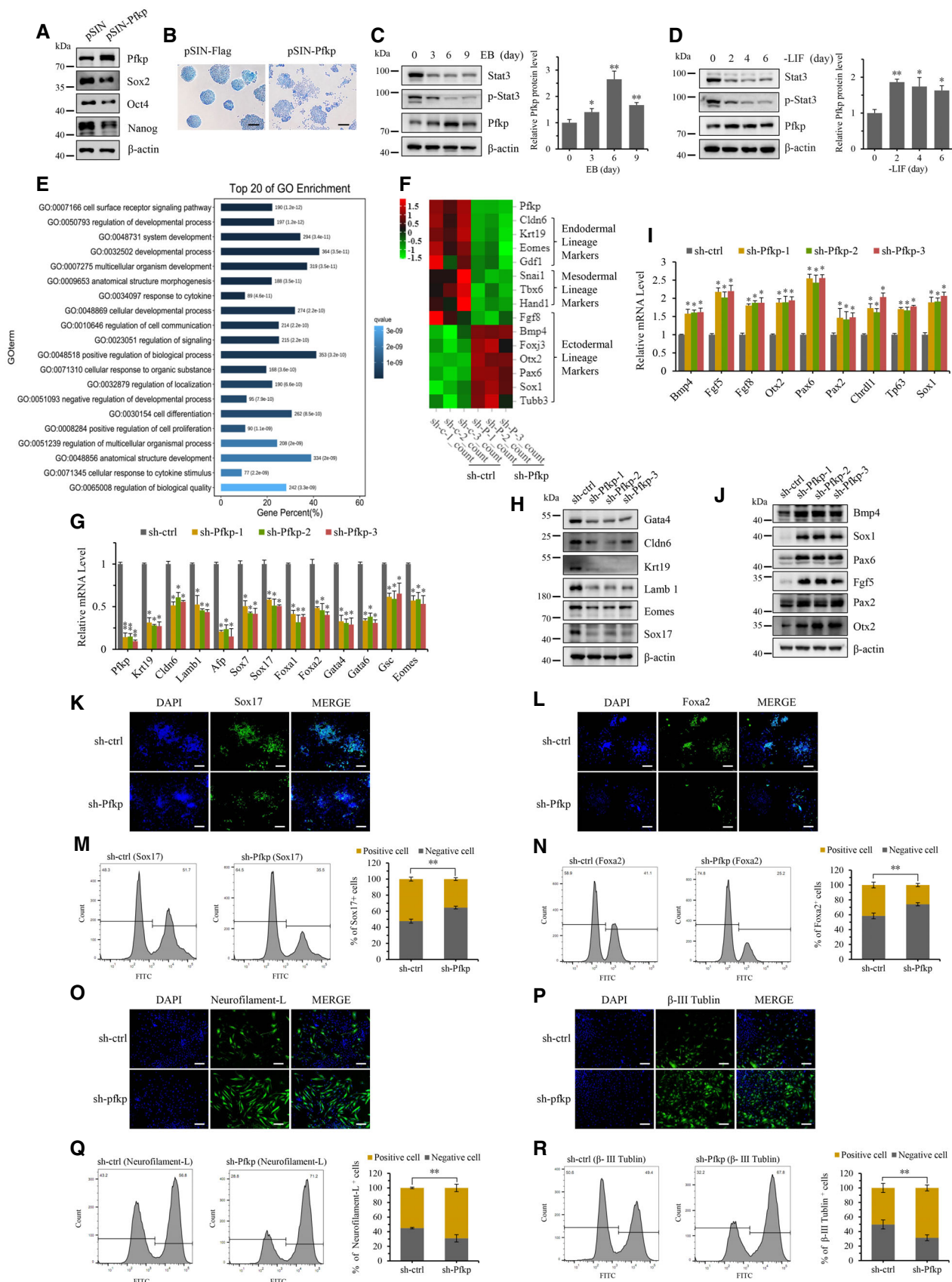
Figure 3.

Figure 3. Pfkp affects mESC differentiation.

A Expression of the pluripotency genes Sox-2, Oct-4, and Nanog in R1 cells after overexpression of Pfkp, as measured by Western blot. β-actin was employed as a loading control throughout.

B Representative images of alkaline phosphatase-stained colonies formed by R1 cells after overexpression of Pfkp. Images were representative of three independent experiments. Scale bar: 200 μm.

C, D Expression of the phosphorylated and total Stat3 and Pfkp in R1 cells as embryoid bodies (EBs) (C) or after withdrawal of LIF (D), as measured by Western blot.

E GO analysis of RNA-seq data of Day 6 control versus Pfkp knockdown EBs.

F Heatmap comparing the expression of lineage specification markers in Day 6 control versus Pfkp knockdown EBs as determined by RNA-seq analysis. Results represent three independent analyses of one shRNA targeting Pfkp and one control shRNA sample.

G, H Expression of endodermal markers in Pfkp knockdown and control EBs at Day 6 determined by qPCR (G) and Western blot (H), respectively.

I, J Expression of ectodermal markers in Pfkp knockdown and control EBs at Day 6 determined by qPCR (I) and Western blot (J), respectively.

K, L Representative images of immunofluorescence staining in control and Pfkp knockdown R1 cells for Sox17 following definitive endoderm differentiation (K) or Foxa2 following definitive endoderm differentiation (L). Green staining indicates positive cells with nuclei counterstained with DAPI. Images were representative of three independent experiments. Scale bar: 200 μm.

M, N Quantitative analysis of Sox17 (M) and Foxa2 (N) in R1 cells from (K) and (L), respectively, as determined by flow cytometry. Representative profiles (left panels) and quantitation (right panels) as a percentage of total cells.

O, P Representative images of immunofluorescence staining in control and Pfkp knockdown R1 cells for Neurofilament-L following neural differentiation (O) or alternatively β-III Tubulin (P). Images were representative of three independent experiments. Scale bar: 200 μm.

Q, R Quantitative analysis of Neurofilament-L (Q) and β-III Tubulin (R) in R1 cells from (O) and (P), respectively, as determined by flow cytometry. Representative profiles (left panels) and quantitation (right panels) as a percentage of total cells.

Data information: The data were repeated three times and shown as the mean ± SD of three independent experiments. One asterisk and two asterisks indicate $P < 0.05$ and $P < 0.01$, respectively.

Lin41. Two prominent phosphopeptides were detected involving serine residues 174 and 800, located at the N- and C-terminals of Lin41, respectively (Fig 5D and Appendix Fig S3G). Moreover, an antibody produced to specifically recognize the Ser174 phosphorylated form of Lin41 provides independent evidence that Pfkp catalyzes Lin41 phosphorylation (Fig 5E). On this basis, S174A and a control S800A Lin41 mutants were constructed to determine the impact of Pfkp phosphorylation on Lin41 polyubiquitination. Notably, ectopic expression of Pfkp diminished wildtype and S800A mutant Lin41 polyubiquitination, whereas basal polyubiquitination in the S174A mutant was reduced and not influenced by Pfkp expression (Fig 5F). Building upon these findings, the polyubiquitination of wildtype and S800A mutant Lin41 was enhanced when endogenous Pfkp expression was silenced in mESCs, although this phenotype was not observed using the S174A mutant (Fig 5G). Reconstituting the Pfkp-Lin41 interactions in vitro showed that recombinant wildtype Lin41 underwent self-catalyzed polyubiquitination that was inhibited by prior incubation with Pfkp, whereas the polyubiquitination of S174A Lin41 mutant was not impacted under the same assay conditions (Fig 5H). Synthesizing the concepts linking Pfkp-mediated phosphorylation with Lin41 polyubiquitination and protein survival, we observed the S174A mutant showed a shorter half-life compared with either wildtype or S800A mutant Lin41 (Fig 5I). Together, these experiments establish that Pfkp-mediated phosphorylation of Lin41 prevents the turnover of Lin41 by inhibiting its autoubiquitination and proteasomal destruction.

Lin41 regulates mESC differentiation by interacting with ectodermal gene mRNAs

Given our preceding findings that Pfkp affects the expression of lineage specification genes, we next compared Lin41-knockdown and control mESCs to study the relationship between Pfkp regulation of Lin41 and lineage differentiation. The levels of pluripotent markers were not affected by Lin41 silencing (Appendix Fig S4A). The transcriptome analysis showed that many biological processes related to

development and differentiation were also discovered to be listed among the top 20 Gene Ontology terms (Fig 6A), and Lin41 knockdown upregulated a group of ectodermal specification genes while suppressing the expression of many mesendodermal specification genes (Fig 6B). These findings were validated by qPCR and Western blot analyses (Fig 6C–E), and in ectodermal cells the levels of Pfkp and Lin41 was indeed lower than those in endodermal differentiating cells (Appendix Fig S4B), providing evidence that Lin41 like Pfkp, favors the expression of endodermal genes over ectodermal genes. However, the underlying mechanism was unclear.

Since the RNA-binding function of Lin41 is known to negatively regulate mRNA expression (Aeschimann et al, 2017), we hypothesized that selective interactions between Lin41 and ectodermal gene mRNAs could account for observed gene expression changes. Towards this, RNA immunoprecipitation (RIP) assays were conducted in mESCs against ectopically expressed 3 × Flag-Lin41 showed that a group of ectodermal gene mRNAs was enriched with Lin41 while other mRNAs associated with endoderm differentiation were largely not recovered (Fig 6F). Furthermore, RNA pulldown assays confirmed the binding between endogenous Lin41 and mRNAs encoding the ectodermal specification genes Fgf5, Otx2, Sox1, and Pax2 (Fig 6G–J). To then verify that Lin41 binding interactions lead to the downregulation of the interacting mRNAs, we assessed mRNA half-lives using actinomycin D chase assays in mESCs. We observed that Lin41 silencing enhanced the stability of Fgf5, Otx2, Sox1, and Pax2 mRNAs (Fig 6K) while knockdown of Pfkp phenocopied these changes, which could be reversed to some extent with the overexpression of Lin41 (Fig 6L). Furthermore, we also determined that the RNA-induced silencing complex (RISC) component Ago2 complexed with Lin41 (Rand et al, 2005; Appendix Fig S5A and B) but since Ago2 expression was not influenced by Lin41 (Appendix Fig S5C), this suggests that Lin41-Ago2-RNA complexes were involved in the RNAi-induced downregulation of the ectodermal gene mRNAs.

Collectively, our results provide evidence for a novel regulatory axis that contributes to pluripotency maintenance in mESCs (Fig 7).
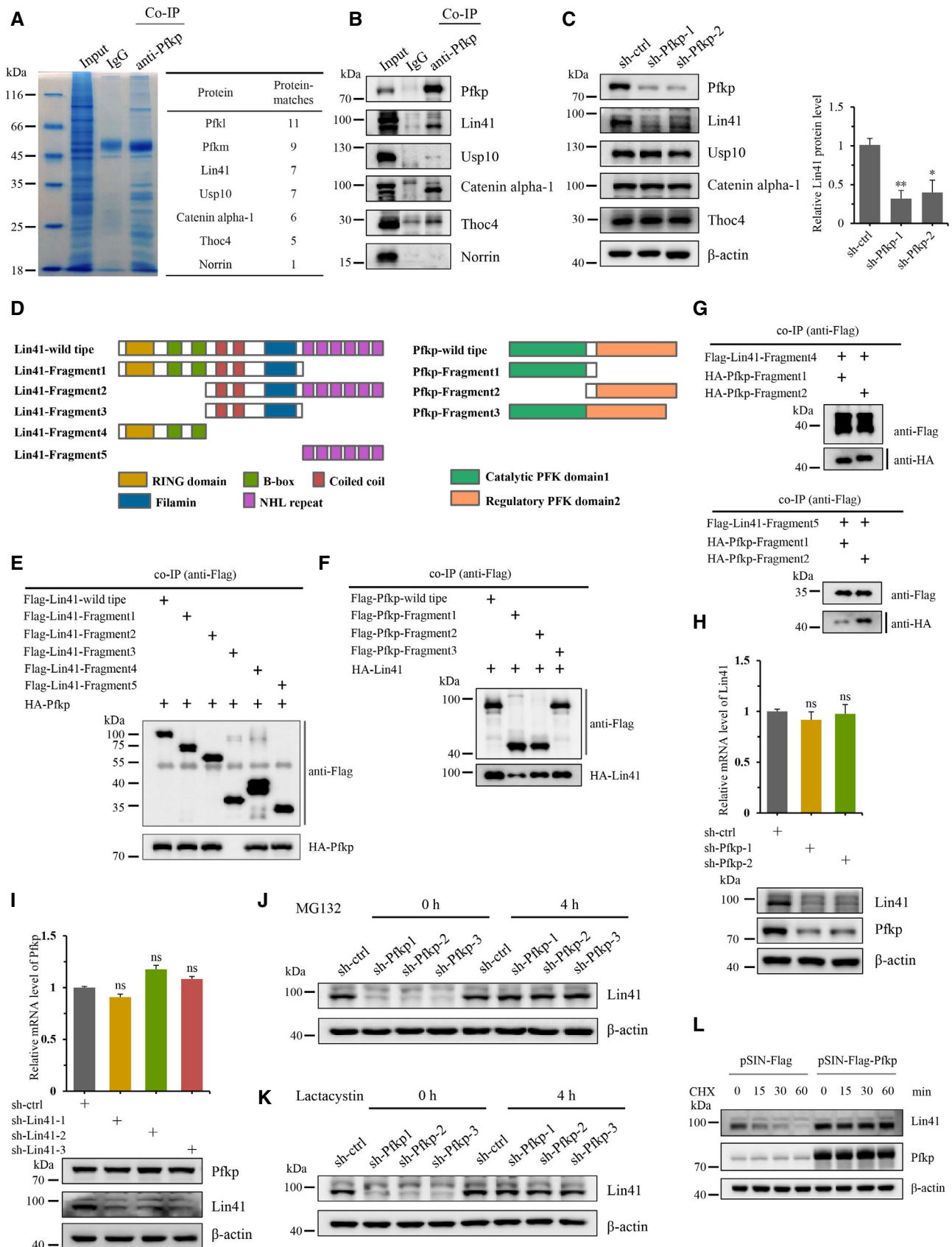
Figure 4.

Figure 4. *Pfkp* interacts with *Lin41* and maintains its stability.

A, B   Protein interactome of Pfkp in R1 cells. SDS–PAGE gel comparing Pfkp and control (IgG) immunoprecipitates (left) with candidate Pfkp-interacting proteins identified by mass spectrometry (right) (A). Validation of candidate Pfkp-interacting proteins using Western blotting (B).

C   Western blot analysis of candidate Pfkp-binding proteins in R1 cells after control (sh-ctrl) or knockdown of Pfkp using two independent shRNAs. β-actin was employed as a loading control throughout.

D   Schematic illustrating the domain organization of the Pfkp and Lin41 proteins with accompanying design of analysis constructs.

E–G   Co-IP assays mapping interactions between Pfkp and fragments of Lin41 (E), interactions between Lin41 and fragments of Pfkp (F) and fragments of Pfkp and Lin41 (G) in HEK293T cells.

H   Lin41 expression in control versus Pfkp knockdown R1 cells determined by qPCR (top) and Western blot (bottom).

I   Pfkp expression in control versus Lin41 knockdown R1 cells determined by qPCR (top) and Western blot (bottom). The data are shown as the mean ± SD of three independent experiments.

J, K   Expression of Lin41 in control versus Pfkp knockdown R1 cells without or with MG132 treatment (J) or with Lactacyctin treatment (K), as determined by Western blot.

L   Protein stability of Lin41 in control versus Pfkp overexpression R1 cells in cycloheximide (CHX) chase assays, as determined by Western blot.

Data information: The data were repeated three times and shown as the mean ± SD of three independent experiments. One asterisk and two asterisks indicate $P < 0.05$ and $P < 0.01$, respectively.

LIF-mediated activation of Stat3 exerts repression of Pfkp transcription, which in turn restrains the expression of Lin41 via an autoubiquitination mechanism. Releasing control over Pfkp permits the Lin41 phosphorylation, which in turn acts to inhibit its ubiquitination and proteasomal turnover. The increased levels of Lin41 then exert regulatory control over key mRNAs involved in the ectodermal specification, favoring the expression of mRNAs determining the endodermal lineage. Thus, our results provide evidence for a hierarchical control mechanism balancing the specification between lineages.

Discussion

Integral relationships exist between cellular energetics and cell fate decisions in ESCs with changes thought to mirror changing cellular requirements (Teslaa & Teitell, 2015). Given the central importance of LIF-Stat3 signaling in ESC pluripotency, we sought to determine whether there was an intersection with glycolysis. Indeed, among the rate-limiting glycolytic isoenzymes, Pfkp was selectively subject to Stat3 regulation but in an unexpected manner. The readout of canonical Stat activation usually involves downstream activation of target genes, whereas Stat3 occupancy at the Pfkp promoter in mESCs was associated with transcriptional repression. Stat proteins can exert repressor effects under both basal and activation states, but this necessitates cooperation with co-repressors such as the NCoR/SMRT complex, which can affect histone modifications (Awasthi *et al*, 2021). While the precise nature of this regulation needs to be confirmed, it was nonetheless evident that depleting Pfkp in mESCs resulted in the upregulation of pluripotency driver genes such as *Sox2*, which is also a repressor of mesendodermal differentiation (Wang *et al*, 2012). Further analyses established that Pfkp could influence germ layer differentiation, specifically its expression served to promote endodermal differentiation in mESCs by antagonizing the expression of ectodermal specification genes. And rather than resulting from the actions of glycolytic metabolites, Pfkp was shown to play a more direct role in this process by its kinase-dependent modulation of the developmental regulator Lin41.

A notable finding was made concerning the specificity shift of Pfkp from a sugar substrate towards protein. During the second priming step of glycolysis, phosphofructokinase catalyzes the phosphorylation of the metabolic intermediate fructose 6-phosphate. The most intuitive explanation for the association of Lin41 with Pfkp was as part of a ubiquitin ligase-substrate recognition complex. Indeed, a prior study showed that TRIM21, another Trim family member, mediates the polyubiquitination and degradation of PFKP (Lee *et al*, 2017). However, Lin41 levels had no bearing on Pfkp expression, and exploring an alternative explanation revealed that the Pfkp-mediated phosphorylation of Lin41 permitted its stabilization via conferring resistance to autoubiquitination and consequent proteasomal turnover. Prior examples of substrate shifts by glycolytic enzymes are rare but have nonetheless been reported, most often involving the two ATP-generating enzymes in the glycolysis pathway, namely PKM2 and PGK1 (Lu & Hunter, 2018). For example, PKM2 phosphorylates H3 histones with this event shown to be a prerequisite for H3 Lys9 acetylation, creating a transcriptionally permissive state for genes including c-Myc and the key cell cycle regulator CCDN1 (Yang *et al*, 2012). Also in the cancer setting, mitochondrial localized PGK1 was shown to directly phosphorylate and activate pyruvate dehydrogenase kinase isozyme 1 (PDK1), thereby constraining mitochondrial respiration by inhibiting pyruvate conversion to acetyl-coA (Li *et al*, 2016). Interestingly, we found at lower substrate concentrations the kinase activity of Pfkp against Lin41 was more efficient than its catalysis of F-6-P phosphorylation. Nonetheless, protein phosphorylation activity peaked and declined, potentially because of recombinant GST-Lin41 protein aggregation. In any event, it is difficult fully relate these findings to physiological conditions given the concentration of F-6-P is 1,000 times greater within cells while the Lin41 concentrations used were higher than cellular levels. Less detailed examples of protein phosphorylation by other glycolytic enzymes are also known, for example, purified HK1 was reported to exhibit kinase activity against histone H2A (Adams *et al*, 1991).

Our data also contribute to the list of examples showing glycolytic enzymes are not solely dedicated to glycolysis (Kim & Dang, 2005; Yu & Li, 2017). Many of these alternative functions involve nuclear roles, where the enzymes act to control gene expression via their inclusion as transcriptional machinery components, either as co-repressors or co-activators. For example, YAP/TAZ target genes mediating breast cancer cell growth were upregulated by the direct binding of PFKM with TEAD transcription factors (Enzo *et al*, 2015) while an alternatively spliced form of α-enolase (ENO1)
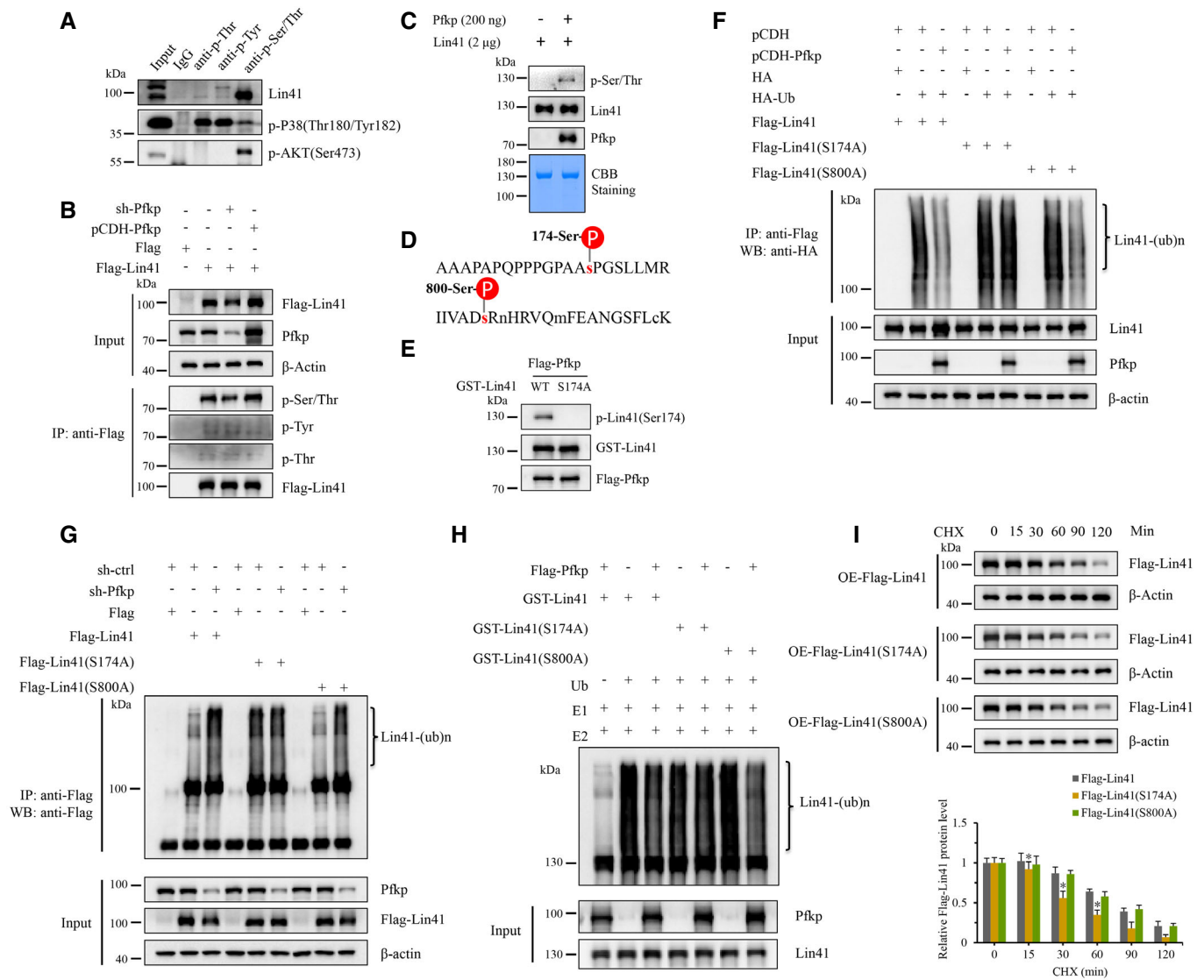
Figure 5. Pfkp catalyzes phosphorylation and inhibits ubiquitination of Lin41.

A Thr, Tyr, or Ser/Thr phosphorylated proteins immunoprecipitated from R1 cells were subjected to Western blot using anti-Lin41, p-p38, and p-Akt antibodies. P-Akt and p-p38 were shown as positive controls.

B The empty Flag vector or Flag-Lin41 was transfected into stable Pfkp knockdown or overexpression R1 cells. Flag immunoprecipitates were analyzed by Western blotting with the pan-specific phosphorylation antibodies (bottom panels) with transfections verified in the input samples (top panels).

C In vitro kinase assays employing recombinant GST-Lin41 and Flag-Pfkp, with phosphorylation of Lin41 measured by Western blotting against pan-specific Ser/Thr phosphorylation antibodies.

D Interpretation of mass spectrometry analysis of Lin41 showing two serine phosphorylated residues.

E In vitro kinase assays as per (C) employing recombinant GST-Lin41 or the GST-Lin41 S174A substitution mutant analyzed by Western blotting using bespoke antibodies raised against phosphorylated Ser 174 in Lin41.

F HEK293T cells were co-transfected with the indicated vectors to overexpress Pfkp in combination with HA-ubiquitin (Ub) and the individual wildtype Flag-Lin41 or serine substitution mutants. Lin41 ubiquitination levels were determined using Western blotting against HA (top panels) with input samples analyzed in parallel to verify transfection efficiency (bottom panels).

G Control or Pfkp knockdown R1 cells were co-transfected with the individual wildtype Flag-Lin41 or serine substitution mutants and Lin41 ubiquitination levels determined as per (F) using Western blotting against Flag.

H In vitro ubiquitination assays employing the products from in vitro kinase assays employing recombinant GST-Lin41 and Flag-Pfkp, with Lin41 ubiquitination measured by Western blotting against Lin41.

I Protein stability of Lin41 in R1 cells overexpressing wildtype Flag-Lin41 or the indicated serine substitution mutants as determined using cycloheximide (CHX) chase assays.

Data information: The data were repeated three times and shown as the mean ± SD of three independent experiments. One asterisk indicates P < 0.05.
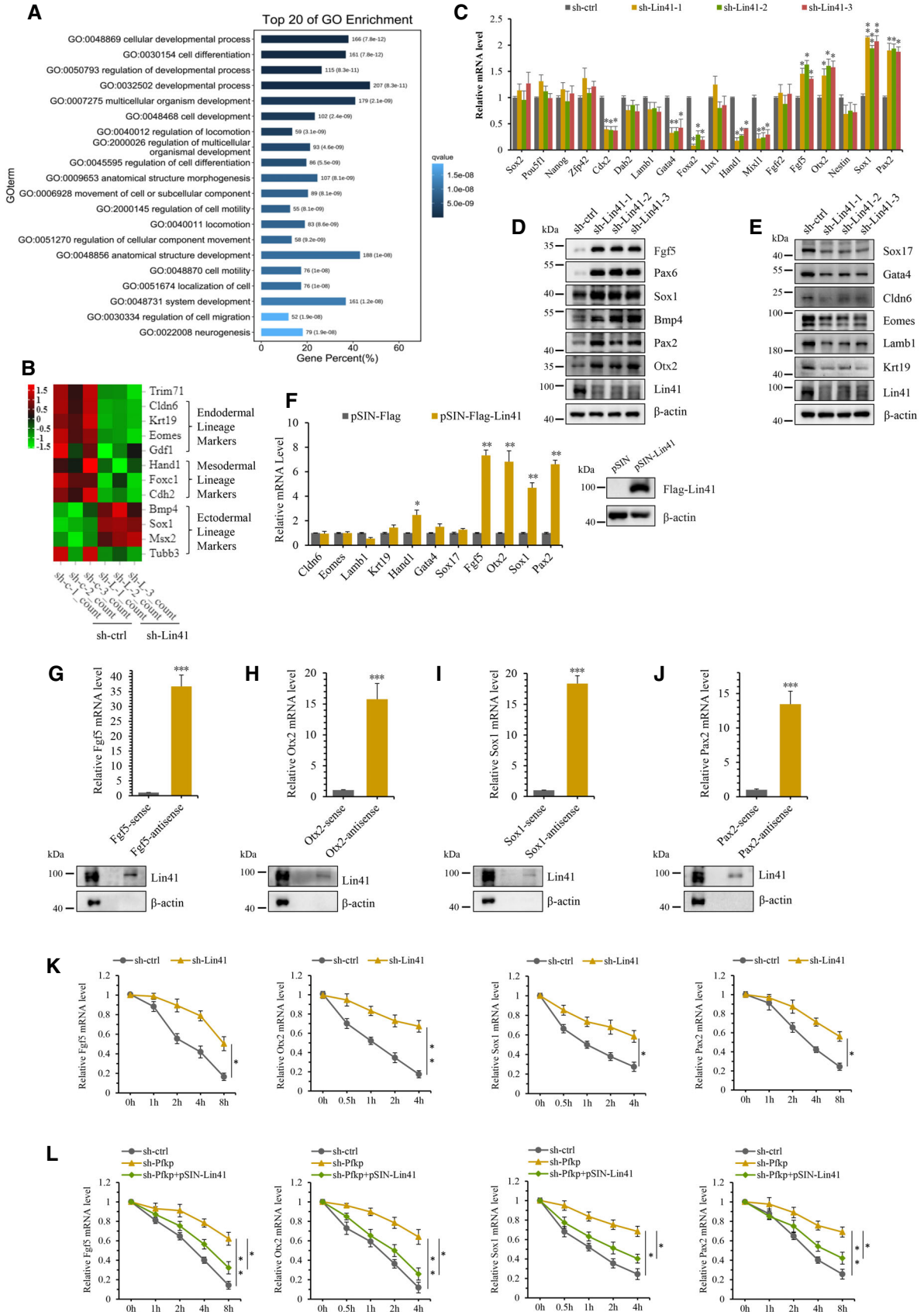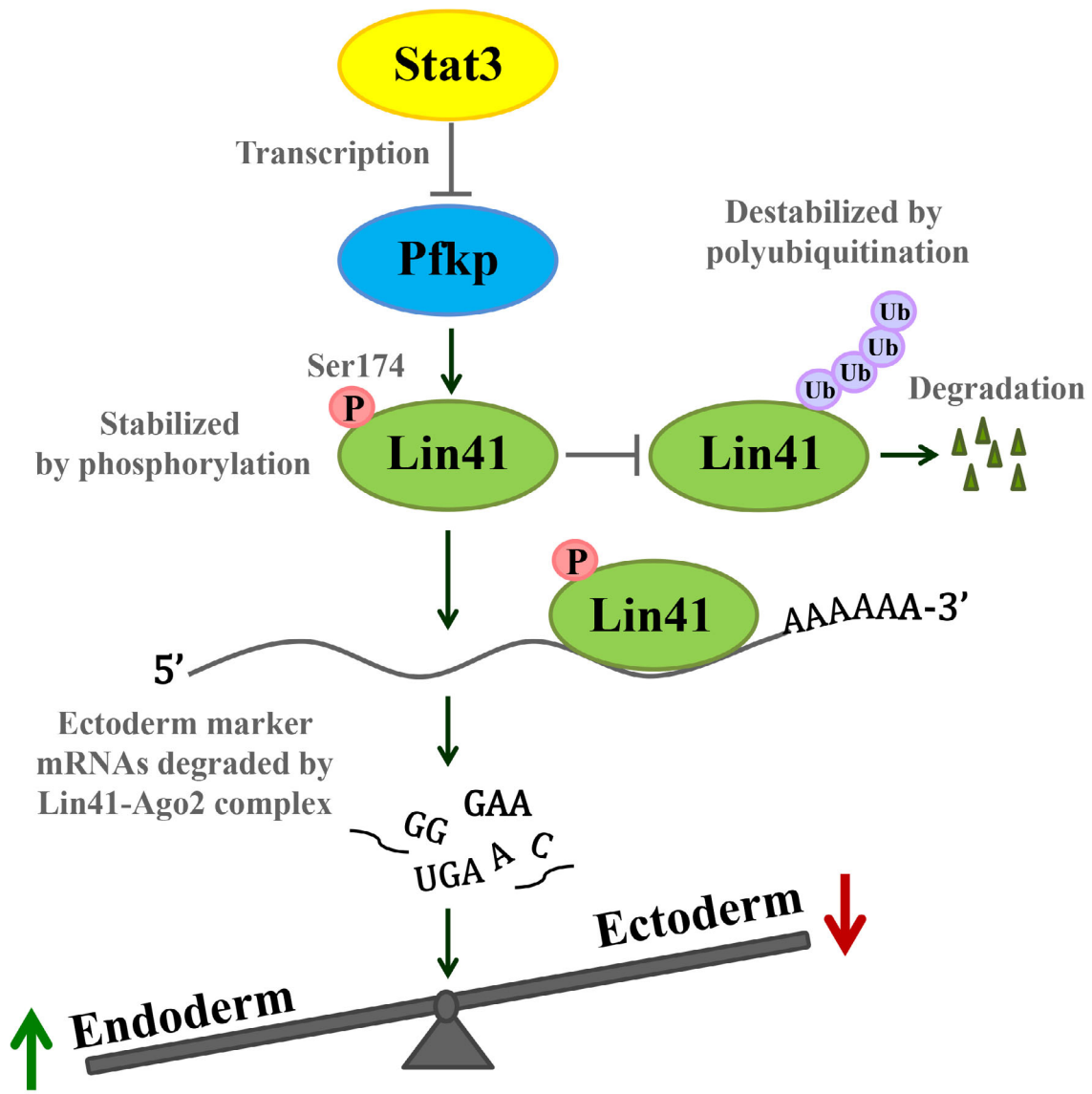
Figure 6.

Figure 6. *Lin41* **interacts with mRNAs of ectoderm genes.**

A   GO analysis of RNA-seq data of Day 6 control versus Lin41 knockdown EBs.
B   Heatmap comparing the expression of lineage specification markers in Day 6 control versus Lin41 knockdown EBs as determined by RNA-seq analysis. Results represent three independent analyses of one shRNA targeting Lin41 and one control shRNA sample.
C–E Expression of selected expression of pluripotency and lineage specification markers in the cells from (B) determined by qPCR (C) with parallel Western blotting analysis of a panel of ectodermal (D) and endodermal (E) markers.
F   RNA immunoprecipitation (RIP) assays in R1 cells measuring interactions between exogenously expressed Lin41 and a panel of ectodermal and endodermal genes, as determined using qPCR. Inset panel shows Western blot validating the expression of Flag-Lin41.
G–J RNA pull-down assays measuring interactions between Fgf5 (G), Otx2 (H), Sox1 (I), and Pax2 (J) mRNAs and endogenous Lin41 in R1 cells. Recovery of each mRNA was compared in sense and antisense probes using qPCR (top) with Western blotting used to detect Lin41(bottom).
K   Relative stability of mRNAs for the ectodermal genes Fgf5, Otx2, Sox1, and Pax2 R1 cells in control and Pfkp knockdown EBs at Day 6, as determined in actinomycin D chase assays.
L   Relative stability of ectodermal gene mRNAs measured as per (K) in Day 6 Pfkp knockdown EBs transfected with or without Lin41.

Data information: The data were repeated three times and shown as the mean ± SD of three independent experiments. One asterisk, two asterisks, and three asterisks indicate $P < 0.05$, $P < 0.01$, and $P < 0.001$, respectively.

Figure 7.   Working model of Pfkp involvement in regulating embryonic stem cell differentiation.

directly acts at the c-Myc promoter as a repressor (Feo et al, 2000). It is relevant to note that it is not presently clear whether these functions inherently rely on enzymatic activity. Nonetheless, the linkage of Pfkp enzymatic activity to mRNA stability, presumably a cytoplasmic process, provides a novel mechanism aspect to this phenomenon.

Interestingly, mapping analysis of the Pfkp-Lin41 interaction then uncovered further unexpected findings. Regions at both ends of Lin41 bound to Pfkp and each half of the Pfkp protein interacted with Lin41. Trim proteins form antiparallel homodimers or heterodimers (Li et al, 2014; Sanchez et al, 2014), and Pfkp is known to assemble as a tetramer (Webb et al, 2015). Thus, it appears implicit that a higher-order oligomeric structure occurs between Pfkp and Lin41 with the different interactions reflecting multiple binding surfaces. Indeed, among these interactions, Pfkp binding to the N-terminal RING domain of Lin41 may contribute to the mechanism whereby Pfkp prevents Lin41 autoubiquitination. However, this speculation requires further clarification, and it similarly needs to be resolved whether RNA binding occurs in the context of the Pfkp-Lin41 complex.

A follow-on question involves how Lin41 specifically recognizes different mRNAs and also how those mRNAs are ultimately repressed. Lin41 enacts translational repression or mRNA degradation in C. elegans, according to its binding preferences to the 5′ or 3′ UTR region, respectively (Aeschimann et al, 2017). And although some examples report translational repression in murine ESCs (Worringer et al, 2014), a global analysis concluded that Lin41 predominately served to degrade target mRNAs with recognition occurring through 3′-UTR binding (Welte et al, 2019). It has been further shown that Lin41 binding involves the recognition of conserved hairpin motifs in target mRNAs with the degree of inhibition dependent on the number of these sites in individual transcripts (Welte et al, 2019). Notably, such motifs are mostly found in 3′-UTR of the downregulated ectodermal-related gene transcripts analyzed in this study, and presumably, this aligns with the 3′-UTR mRNA-binding model involving transcript destabilization. However, the mode by which Lin41 reduces target RNA transcript abundance is less clear.

Specific examples have linked the mRNA repressor function of Lin41 with RISC activity. During murine ESC self-renewal, Cdkn1a transcripts are destabilized by Lin41 in cooperation with miR-302 with Trim71 shown to associate with Ago2 and localize to cytoplasmic processing (P) bodies (Chang et al, 2012). Moreover, other studies have reported a physical association between Lin41 and different components of the RISC including different isoforms of Ago and Pum proteins (Loedige et al, 2013; Torres-Fernandez et al, 2019) although this appears not to be a universal explanation for Lin41 function since functional others have found that Trim71 repression is independent of Ago proteins (Loedige et al, 2013, Torres-Fernandez et al, 2019). Indeed, a subset of TRIM71/Lin41 target mRNAs including CDKN1A was destabilized independently of RISC-mediated silencing through nonsense-mediated decay machinery (Torres-Fernandez et al, 2019). Based on precedents observed with other Trim family members, it was proposed that Lin41 likely exercises combinatorial control over RNA metabolism alone or in cooperation with other mechanisms (Connacher & Goldstrohm, 2021).

Finally, we must consider the relative importance of Pfkp to the control of Lin41 expression and function during its regulation of lineage commitment. Notably, we found a good correlation between

the Pfkp-mediated stabilization of Lin41, and its binding and down-regulation of ectodermal gene mRNAs while endodermal gene expression was upregulated. Moreover, our findings align with the global gene expression changes identified in Trim71 knockout mESCs where ectodermal specification genes were upregulated (Mitschka et al, 2015). Furthermore, our observations are consistent with the "seesaw" model, which claims that lineage specifiers direct ESC differentiation into a specific germ layer while cross-inhibiting commitment to mutually exclusive lineages (Shu et al, 2013). Coincident with this theory, we ascribed the repressed mesendoderm formation to the enhanced expression of ectodermal factors in Pfkp knockdown cells (refer Fig 7). Nonetheless, comparisons between ESCs following Pfkp and Lin41 silencing revealed differences in the levels of pluripotency and lineage markers. We propose the role of Pfkp in promoting differentiation is dynamic in different stages. After differentiation starts, as ectodermal gene expressions are upregulated, the function of Pfkp is inhibiting ectodermal markers and directing differentiation into certain lineages by regulating Lin41. However, in naïve stem cells, the role of Pfkp is accelerating stem cells leaving pluripotency, and no significant phenotype after Lin41 KD was detected by us in mESCs. We propose that Lin41 only mediates the effect of Pfkp once differentiation starts and inhibits entering ectodermal lineage, while in the naïve state, there are unknown factors working downstream of Pfkp, which needs further investigation.

Taken together, our study uncovers the role of the LIF-Stat3-Pfkp-Lin41 pathway during early embryonic development and proposes practical implications for modulating germ layer differentiation in vitro.

Materials and Methods

Reagents and antibodies

Reagents and antibodies are shown in Appendix Tables S1 and S2; Oligonucleotide sequences related to Figures are shown in Appendix Tables S3–S6; Recombinant DNA used is shown in Appendix Table S7. Rabbit polyclonal antibodies recognizing Ser174 phosphorylated Lin41 were custom prepared by PTM Biolabs (Hangzhou, China) using the peptide CQPPPGPAA-(phospho)SPGSL as immunogen. The serum from three immunized rabbits was first depleted against an affinity column conjugated with unmodified peptides before affinity purifying the specific antibodies over a column conjugated with the phosphorylated peptide. After elution, the antibodies were eluted and concentrated before evaluating specificity using immunoblotting in presence of blocking peptides.

Cell culture

Mouse R1 ES cells (ATCC, SCRC-1011™) and E14 cells were cultured in DMEM supplemented with 15% fetal bovine serum, 2 mM L-glutamine, 100 mM nonessential amino acids, 0.1 mM β-mercaptoethanol, 1 mM sodium pyruvate (Gibco) and 1,000 U/ml LIF (Millipore) on gelatin-coated plates. Mouse ES cell culture media (2i media): 2 μM PD0325901 and 3 μM CHIR99021 were supplemented into a 1:1 mix of DMEM/F12 and Neurobasal medium containing N2 (1:100 dilutions) and B27 supplements (1:50 dilutions),

7.5% BSA, 2 mM L-glutamine. Alternatively, HEK293T cells were cultured in DMEM supplemented with 10% fetal bovine serum, 1 mM sodium pyruvate, and 100 mg/ml streptomycin (Gibco). All cell lines were authenticated with short tandem repeat assays and tested negative for Mycoplasma contamination.

Lentivirus packaging and infection

To generate lentiviruses expressing shRNAs, HEK293T cells were co-transfected with shRNA or control vector (cloned in pLKO.1), pREV, pGag/Pol, and pVSVG at the ratio of 2:2:2:1. To generate lentiviruses expressing indicated proteins, HEK293T cells were co-transfected with pCDH/pSIN-based construct, pMD2.G, and psPAX2 at the ratio of 2:1:2. Twelve hours after transfection, cells were changed for fresh medium and cultured for an additional 24 h. The culture medium containing lentivirus particles was collected and filtered through a 0.45 μm polyvinylidene difluoride filter (Millipore) and incubated with 4 μg/ml polybrene (Sigma) for 12 h, followed by selection with 5 μg/ml puromycin for another 24 h.

qPCR

Total RNA was extracted using Trizol (Invitrogen). One microgram of total RNA was used for cDNA synthesis with a PrimeScriptTM RT reagent kit (Takara) according to the instruction provided by the manufacturer. qPCR was performed using Universal SYBR real-time PCR analysis (Takara) and analyzed with LightCycler96 (Roche).

Western blotting

Western blotting was performed as described before. Briefly, cells were harvested, boiled in an SDS loading buffer, and separated by SDS–PAGE. Proteins were transferred onto nitrocellulose membrane (Bio-Rad) and detected by indicated primary antibody and HRP-conjugated secondary antibody. Protein bands were quantified by ImageJ software.

Co-Immunoprecipitation assay

Briefly, cells were harvested and lysed in IP lysis buffer (0.5% NP-40, 150 mM NaCl, 20 mM HEPES, pH 7.5, 2 mM EDTA, and 1.5 mM $MgCl_2$) supplemented with protease inhibitor cocktail for 30 min on ice. Cell lysates were incubated with protein A/G-sepharose beads coated with the indicated antibodies at 4°C for 4 h. The immunoprecipitates were then subjected to Western blot analysis.

ChIP assays

Assays were performed using the ChIP Assay Kit (CST) according to the manufacturer's instructions. Briefly, approximately 1×10^7 cells in suspension were cross-linked for 15 min at 37°C in 1% formaldehyde before quenching with glycine (0.125 M) for 5 min at room temperature. After pelleting by centrifugation, the cells were then lysed in 300 μl SDS lysis buffer (50 mM Tris–HCl (pH 8.0), 10 mM EDTA, 0.5% SDS, and protease inhibitors) for 15 min on ice before sonication to generate DNA fragments approximately 200–1,000 bp

in size. The lysates were then subjected to immunoprecipitation with antibodies against STAT3 or p-STAT3 (Y705) overnight before sequential washes with low-salt buffer, high-salt buffer, LiCl salt buffer, and TE buffer. Histone–DNA complexes were eluted using elution buffer (1% SDS and 0.1 M NaHCO₃) and incubated at 65°C overnight in the presence of 0.25 M NaCl. The next day, DNase-free RNase (10 mg/ml) was added to the samples and incubated for 1 h at 37°C before further incubation with Proteinase K for another 1 h at 55°C. The eluted DNA was purified by phenol-chloroform extraction and ethanol precipitation and DNA fragments subjected to semiquantitative PCR using the specified primers (Appendix Table S5).

Luciferase reporter assay

The DNA fragments containing potential STAT3-binding sequence were amplified by PCR and then cloned into pGL3-Basic vector (Promega). HEK293T cells were transfected with the indicated plasmids. The relative luciferase activities were calculated by normalizing the firefly luciferase activity to Renilla luciferase activity.

Rip

Briefly, 1×10^7 cells were lysed in cell lysis buffer (0.5% NP-40, 150 mM NaCl, 25 mM Tris [pH 7.4], pH 7.5, 2 mM EDTA, and 1.5 mM $MgCl_2$) supplemented with RNase A inhibitor and DNase I before centrifugation. Cell lysates were incubated with protein A/G beads coated with the indicated antibodies at 4°C for 3 h. After extensive washing, the bead-bound immunocomplexes were eluted using elution buffer (50 mM Tris [pH 8.0], 1% SDS, and 10 mM EDTA) at 65°C for 10 min. The eluted immunocomplexes were treated with proteinase K, and RNAs were extracted by Trizol. Purified RNAs were then subjected to qPCR analysis.

RNA pull-down assays

In brief, all processes were performed in RNase-free conditions. Briefly, approximately 1×10^7 cells were lysed in 1.0 ml of lysis buffer (50 mM Tris–HCl (pH 7.5), 150 mM NaCl, 2.5 mM $MgCl_2$, 1 mM EDTA, 10% glycerol, 0.5% NP-40, 1 mM DTT), supplemented with RNase Inhibitor (Thermo Fisher Scientific) and Protease Inhibitor Mixture (Roche). Cell lysates were incubated with streptavidin beads (Invitrogen) coated with the biotin-labeled anti-sense probes (4 μg) at 4°C for 4 h overnight. A biotin-labeled sense probe (4 μg) sample was taken as a negative control. Beads were washed five times in RIP buffer and eluted in Laemmli buffer. The retrieved proteins were separated by SDS–PAGE for Western blotting.

RNA-seq analysis

Control or stable knockdown R1 cells (Pfkp or Lin41) were cultured in low-adsorption 6-well plates in a medium without -LIF for 6 days, and the medium was changed every 2 days. The cells were collected after 6 days, and total RNA was extracted by Trizol before commercial mRNA-seq was performed and analyzed by Gene Denovo Biotechnology Co. (Guangzhou, China). RNA-seq data were mapped to the mouse reference genome (Ensembl104)

using HISAT2 (version 2.2.1). The levels of gene expression were calculated by Cufflinks (version 2.2.1) based on Ensembl 104 annotations. Differential testing and log2 fold change calculations were performed using TE analysis (version 4.6), with the implementation of three biological replicates. The differentially expressed genes (DEGs) were screened using the following criteria: a $|log2FC| > 1$, and a false discovery rate (FDR) < 0.05. GO enrichment analysis of Pfkp or Lin41 target genes based on biological process (BP). X-axis displays a number of differentially expressed genes; Y-axis indicates GO terms. We identified the pluripotent Markers and Lineage Markers through R&D Systems (https://www.rndsystems.com/) whose FDR ≤ 0.05 as well, and then used OmicShare Tools (https://www.omicshare.com/tools/home/soft/getsoft.html) to make a heatmap of these markers after Pfkp and Lin41 knockdown.

Immunofluorescence

Cells were fixed in 4% formaldehyde and permeabilized using 0.1% Triton X-100 followed by blocking with 5% bovine serum albumin, incubation for 1 h at room temperature with primary antibodies before the addition of Alexa Fluor secondary antibodies for 0.5 h at room temperature. Cell nuclei were counterstained by 4′,6-diamidino-2-phenylindole (DAPI), and images were acquired using an Olympus fluorescence microscope.

EB formation assay

Embryoid body was induced by plating mouse ESCs into nonadherent conditions in mES medium lacking LIF for the indicated time.

Neuronal progenitor differentiation assay

Briefly, EBs were plated on gelatin-coated dishes in knockout DMEM containing epidermal growth factor, basic fibroblast growth factor, and L-ascorbic acid. Eight to 24 h later, the medium was replaced by proliferation medium: DMEM/F12 supplemented with 10% FBS, 2 mM L-glutamine, 20 nM progesterone, 100 mM putrescine, 25 mg/ml insulin, 50 mg/ml transferrin, and 30 nM sodium selenite (Gibco; Lau et al, 2006).

Definitive endoderm differentiation assay

Mouse embryonic stem cells (R1 cells) were cultured in suspension for 2 days to form embryoid bodies (EBs). The resulting EBs were transferred onto unwoven polytetrafluoroethylene (PTFE) cloth and treated with FGF-2 (100 ng/ml) and Activin-A (100 ng/ml) for 3–4 days (Soto-Gutierrez et al, 2007).

In vitro kinase assay

HEK293T was transfected with 8 μg of Flag-Pfkp. After 48 h post-transfection, cells were lysed and Flag-Pfkp was immunoprecipitated with anti-Flag M2 affinity beads and then eluted with Flag peptides. Pfkp-Flag (pT7-Pfkp-Flag) and GST-Lin41 wt/S174A/S800A (pGEX-5X-3-Lin41 wt/S174A/S800A) were bacterially purified. The kinase reaction was performed at 37°C for 20 min in the kinase buffer (25 mM Tris–HCl [pH 7.5], 5 mM beta-glycerophosphate,

2 mM dithiothreitol (DTT), 0.1 mM Na_3VO_4, 10 mM $MgCl_2$), supplemented with ATP (100 μM), and the reaction was terminated by adding SDS sample buffer and subjected to SDS–PAGE (Yuan et al, 2019).

In vivo ubiquitination assay

Assays were performed under denaturing conditions as previously described (Tang et al, 2006). Briefly, cells were transfected with the indicated plasmids for 24 h before the addition of 20 μM MG132 for a further 3–6 h. Afterwards, the cells were lysed in SDS lysis buffer (50 mM Tris–HCl, pH 7.4, 150 mM NaCl, 1 mM EDTA, 0.5% sodium deoxycholate, 1% SDS, and 20 μM MG132), supplemented with a protease inhibitor cocktail (Roche). After boiling for 5 min, lysates were diluted 10 times with cold lysis buffer supplemented with protease inhibitors and 10 mM N-ethylmaleimide. Cell lysates were incubated with anti-Flag M2 affinity beads at 4°C for 4 h, and the immunoprecipitates and input were then subjected to Western blot analysis to detect polyubiquitination.

In vitro ubiquitination assay

Assays were performed as previously described with modifications (Tang et al, 2006). The bead-bound GST-Lin41, GST-Lin41-S174A, or GST-Lin41-S180A were phosphorylated by Flag-Pfkp, and the resultant products were then washed and incubated for 1 h at 37°C with 100 nM E1 (UBE1), 1 μM E2 (UbcH5a), 500 μM HA-Ub (Sigma), in ubiquitination buffer (40 mM Tris–HCl at pH 7.4, 2.5 mM Mg^{2+}-ATP, 2 mM DTT). The reactions were terminated by adding an equal amount of 2xSDS loading buffer, boiled, and analyzed by Western blotting.

Mass spectrometry

To identify the phosphorylated amino residues on Lin41, in vitro kinase reactions employing GST-Lin41 in the absence and presence of Pfkp were resolved by SDS–PAGE and stained with Coomassie blue solution. The GST-Lin41 band was excised from the gel and subjected to LC–MS/MS analysis. The resulting MS/MS data were processed using Proteome Discoverer 1.3 with peptide confidence set at high, and peptide ion score set > 20. For identifying potential Pfkp-interacting proteins, cell lysates were collected and incubated with control immunoglobulin G (IgG) or Pfkp preconjugated to A/G beads as described for the immunoprecipitation assays. After SDS–PAGE, the Commassie blue-stained bands of interest were excised and subjected to LC–MS/MS.

Seahorse ECAR glycolysis stress test

Assays were performed using the Seahorse XFe24 analyzer (Agilent) according to the manufacturer's instructions. Briefly, cells were seeded at 3×10^4 cells per well in 24-well XF cell culture gelatin-coated micro-plates for 24 h before performing glycolysis stress tests at 37°C in XF base medium (1 mM glutamine, pH 7.4) with sequential additions of glucose (10 mM), oligomycin (1 μM), and 2-DG (50 mM). Data were analyzed by the Seahorse XF Glycolysis Stress Test Report Generator package.

Measurement of cellular Acetyl-CoA

Measurement of cellular acetyl-CoA levels was performed using an acetyl-CoA fluorometric assay kit (Abcam) following the manufacturer's instructions. Briefly, 2×10^6 cells were homogenized with 100 μl of ice-cold assay buffer for 10 min on ice. The lysates were centrifuged at 10,000 g and 4°C for 10 min, and the supernatant was deproteinized using 10-kD-molecular-weight-cutoff spin columns. After free CoA was quenched, the samples were then mixed with 50 μl of a reaction mixture and incubated at 37°C for 10 min in the dark. The value was measured by fluorescence (excitation/emission = 535/587 nm) using a multidetection microplate reader.

Measurement of Fructose-1,6-Bisphosphate (F1,6BP)

Measurement of F1,6BP levels was performed using the Fructose-1,6-Bisphosphate assay kit (Abcam) following the manufacturer's instructions. Briefly, 2×10^6 cells were homogenized with 500 μl of ice-cold F1,6BP and placed on ice for 10 min. The lysates were centrifuged at 10,000 g and 4°C for 10 min, and the supernatant was used 10-kD-molecular-weight-cutoff spin columns to remove any possible interfering enzymes and insoluble components. The samples were then mixed with 50 μl of a reaction mix and incubated at 37°C for 40 min protected from light. Measure the fluorescence of all wells at Ex/Em = 535/587 nm in endpoint mode.

Measurement of ADP

Measurement of ADP was performed using an ADP-Glo™ Kinase Assay kit (Promega) following the manufacturer's instructions. Briefly, equal volumes of the ADP-Glo™ Reagent were added for 40 min at room temperature to stop kinase activity and deplete any unconsumed ATP to leave only ADP. Afterwards, kinase detection reagent was added at room temperature for 30 min to convert ADP to ATP with ATP levels measured by luciferase-luciferin reactions measured as luminescence using a plate-reading luminometer.

Quantification of Pfkl, Pfkm, and Pfkp proteins

Flag-Pfkl, Flag-Pfkm, and Flag-Pfkp were expressed in HEK293T cells and purified using Flag-M2 beads. The proteins were eluted using Flag peptides and quantified by BCA Protein Assay KIT (Beyotime). The levels of Pfkl, Pfkm, and Pfkp in 5×10^4 R1 cells were analyzed by Western blot along with the purified Pfkl, Pfkm, and Pfkp protein standards with results reported from three independent experiments.

Reproducibility

All the data were repeated at least three times, and at least three sample size was chosen to detect a prespecified effect size. The western blot analyses were representative of three independent experiments. For experiments using cell lines, there was no human bias given all data were collected independently using instrumentation.

Statistical analysis

Analysis was performed using Microsoft Excel and Graph Pad Prism to assess differences between varying groups. Statistical significance was defined by the Student's t-test and expressed as a P-value. P-values < 0.05 were considered to be statistical significance.

Data availability

RNA-sequencing data have been deposited at NCBI GEO under accession numbers GSE216394 (https://www.ncbi.nlm.nih.gov/geo/), and the mass spectrometry proteomic data have been deposited at ProteomeXchange Consortium with the dataset identifier PXD038944 (https://www.ebi.ac.uk/pride).

Expanded View for this article is available online.

Author contributions

Mian Wu: Conceptualization; resources; supervision; funding acquisition; writing – original draft; project administration; writing – review and editing. **Leixi Cao:** Validation; investigation; visualization; writing – original draft. **Ruijie Wang:** Validation; investigation; visualization. **Guangzhi Liu:** Resources; supervision. **Yuwei Zhang:** Resources; supervision. **Rick Francis Thorne:** Writing – original draft; writing – review and editing. **Xu Dong Zhang:** Resources; supervision. **Jinming Li:** Resources; supervision. **Yang Xia:** Resources. **Lili Guo:** Resources. **Fengmin Shao:** Resources; supervision. **Hao Gu:** Conceptualization; writing – original draft; project administration; writing – review and editing.

Disclosure and competing interests statement

The authors declare that they have no conflict of interest.

References

Adams V, Griffin LD, Gelb BD, McCabe ERB (1991) Protein kinase activity of rat brain hexokinase. *Biochem Biophys Res Commun* 177: 1101–1106

Aeschimann F, Kumari P, Bartake H, Gaidatzis D, Xu L, Ciosk R, Grosshans H (2017) LIN41 post-transcriptionally silences mRNAs by two distinct and position-dependent mechanisms. *Mol Cell* 65: 476–489

Awasthi N, Liongue C, Ward AC (2021) STAT proteins: a kaleidoscope of canonical and non-canonical functions in immunity and cancer. *J Hematol Oncol* 14: 198

Boyer LA, Lee TI, Cole MF, Johnstone SE, Levine SS, Zucker JP, Guenther MG, Kumar RM, Murray HL, Jenner RG *et al* (2005) Core transcriptional regulatory circuitry in human embryonic stem cells. *Cell* 122: 947–956

Chambers I, Colby D, Robertson M, Nichols J, Lee S, Tweedie S, Smith A (2003) Functional expression cloning of Nanog, a pluripotency sustaining factor in embryonic stem cells. *Cell* 113: 643–655

Chang HM, Martinez NJ, Thornton JE, Hagan JP, Nguyen KD, Gregory RI (2012) Trim71 cooperates with microRNAs to repress Cdkn1a expression and promote embryonic stem cell proliferation. *Nat Commun* 3: 923

Chen J, Lai F, Niswander L (2012) The ubiquitin ligase mLin41 temporally promotes neural progenitor cell maintenance through FGF signaling. *Genes Dev* 26: 803–815

Cliff TS, Wu T, Boward BR, Yin A, Yin H, Glushka JN, Prestegaard JH, Dalton S (2017) MYC controls human pluripotent stem cell fate decisions through regulation of metabolic flux. *Cell Stem Cell* 21: 502–516

Connacher RP, Goldstrohm AC (2021) Molecular and biological functions of TRIM-NHL RNA-binding proteins. *Wiley Interdiscip Rev RNA* 12: e1620

Darnell JE Jr, Kerr IM, Stark GR (1994) Jak-STAT pathways and transcriptional activation in response to IFNs and other extracellular signaling proteins. *Science* 264: 1415–1421

Do DV, Ueda J, Messerschmidt DM, Lorthongpanich C, Zhou Y, Feng B, Guo G, Lin PJ, Hossain MZ, Zhang W *et al* (2013) A genetic and developmental pathway from STAT3 to the OCT4-NANOG circuit is essential for maintenance of ICM lineages in vivo. *Genes Dev* 27: 1378–1390

Enzo E, Santinon G, Pocaterra A, Aragona M, Bresolin S, Forcato M, Grifoni D, Pession A, Zanconato F, Guzzo G *et al* (2015) Aerobic glycolysis tunes YAP/TAZ transcriptional activity. *EMBO J* 34: 1349–1370

Evans MJ, Kaufman MH (1981) Establishment in culture of pluripotential cells from mouse embryos. *Nature* 292: 154–156

Feo S, Arcuri D, Piddini E, Passantino R, Giallongo A (2000) ENO1 gene product binds to the c-myc promoter and acts as a transcriptional repressor: relationship with Myc promoter-binding protein 1 (MBP-1). *FEBS Lett* 473: 47–52

Fu XY, Kessler DS, Veals SA, Levy DE, Darnell JE Jr (1990) ISGF3, the transcriptional activator induced by interferon alpha, consists of multiple interacting polypeptide chains. *Proc Natl Acad Sci USA* 87: 8555–8559

Fu XY, Schindler C, Improta T, Aebersold R, Darnell JE Jr (1992) The proteins of ISGF-3, the interferon alpha-induced transcriptional activator, define a gene family involved in signal transduction. *Proc Natl Acad Sci USA* 89: 7840–7843

Gu W, Gaeta X, Sahakyan A, Chan AB, Hong CS, Kim R, Braas D, Plath K, Lowry WE, Christofk HR (2016) Glycolytic metabolism plays a functional role in regulating human pluripotent stem cell state. *Cell Stem Cell* 19: 476–490

Hall J, Guo G, Wray J, Eyres I, Nichols J, Grotewold L, Morfopoulou S, Humphreys P, Mansfield W, Walker R *et al* (2009) Oct4 and LIF/Stat3 additively induce Kruppel factors to sustain embryonic stem cell self-renewal. *Cell Stem Cell* 5: 597–609

Jain AK, Allton K, Duncan AD, Barton MC (2014) TRIM24 is a p53-induced E3-ubiquitin ligase that undergoes ATM-mediated phosphorylation and autodegradation during DNA damage. *Mol Cell Biol* 34: 2695–2709

Kim JW, Dang CV (2005) Multifaceted roles of glycolytic enzymes. *Trends Biochem Sci* 30: 142–150

Kim H, Jang H, Kim TW, Kang BH, Lee SE, Jeon YK, Chung DH, Choi J, Shin J, Cho EJ *et al* (2015) Core pluripotency factors directly regulate metabolism in embryonic stem cell to maintain pluripotency. *Stem Cells* 33: 2699–2711

Kwon SC, Yi H, Eichelbaum K, Fohr S, Fischer B, You KT, Castello A, Krijgsveld J, Hentze MW, Kim VN (2013) The RNA-binding protein repertoire of embryonic stem cells. *Nat Struct Mol Biol* 20: 1122–1130

Lau T, Adam S, Schloss P (2006) Rapid and efficient differentiation of dopaminergic neurons from mouse embryonic stem cells. *Neuroreport* 17: 975–979

Lee JH, Liu R, Li J, Zhang C, Wang Y, Cai Q, Qian X, Xia Y, Zheng Y, Piao Y *et al* (2017) Stabilization of phosphofructokinase 1 platelet isoform by AKT promotes tumorigenesis. *Nat Commun* 8: 949

Li Y, Wu H, Wu W, Zhuo W, Liu W, Zhang Y, Cheng M, Chen YG, Gao N, Yu H *et al* (2014) Structural insights into the TRIM family of ubiquitin E3 ligases. *Cell Res* 24: 762–765

Li X, Jiang Y, Meisenhelder J, Yang W, Hawke DH, Zheng Y, Xia Y, Aldape K, He J, Hunter T *et al* (2016) Mitochondria-translocated PGK1 functions as a protein kinase to coordinate glycolysis and the TCA cycle in tumorigenesis. *Mol Cell* 61: 705–719

Liu Q, Chen X, Novak MK, Zhang S, Hu W (2021) Repressing Ago2 mRNA translation by Trim71 maintains pluripotency through inhibiting let-7 microRNAs. *Elife* 10: e66288

Loedige I, Gaidatzis D, Sack R, Meister G, Filipowicz W (2013) The mammalian TRIM-NHL protein TRIM71/LIN-41 is a repressor of mRNA function. *Nucleic Acids Res* 41: 518–532

Lu Z, Hunter T (2018) Metabolic kinases moonlighting as protein kinases. *Trends Biochem Sci* 43: 301–310

Martin GR (1981) Isolation of a pluripotent cell line from early mouse embryos cultured in medium conditioned by teratocarcinoma stem cells. *Proc Natl Acad Sci USA* 78: 7634–7638

Mitschka S, Ulas T, Goller T, Schneider K, Egert A, Mertens J, Brustle O, Schorle H, Beyer M, Klee K *et al* (2015) Co-existence of intact stemness and priming of neural differentiation programs in mES cells lacking Trim71. *Sci Rep* 5: 11126

Mitsui K, Tokuzawa Y, Itoh H, Segawa K, Murakami M, Takahashi K, Maruyama M, Maeda M, Yamanaka S (2003) The homeoprotein Nanog is required for maintenance of pluripotency in mouse epiblast and ES cells. *Cell* 113: 631–642

Moussaieff A, Rouleau M, Kitsberg D, Cohen M, Levy G, Barasch D, Nemirovski A, Shen-Orr S, Laevsky I, Amit M *et al* (2015) Glycolysis-mediated changes in acetyl-CoA and histone acetylation control the early differentiation of embryonic stem cells. *Cell Metab* 21: 392–402

Nguyen DTT, Richter D, Michel G, Mitschka S, Kolanus W, Cuevas E, Wulczyn FG (2017) The ubiquitin ligase LIN41/TRIM71 targets p53 to antagonize cell death and differentiation pathways during stem cell differentiation. *Cell Death Differ* 24: 1063–1078

Nichols J, Zevnik B, Anastassiadis K, Niwa H, Klewe-Nebenius D, Chambers I, Scholer H, Smith A (1998) Formation of pluripotent stem cells in the mammalian embryo depends on the POU transcription factor Oct4. *Cell* 95: 379–391

Niwa H, Burdon T, Chambers I, Smith A (1998) Self-renewal of pluripotent embryonic stem cells is mediated via activation of STAT3. *Genes Dev* 12: 2048–2060

Rand TA, Petersen S, Du F, Wang X (2005) Argonaute2 cleaves the anti-guide strand of siRNA during RISC activation. *Cell* 123: 621–629

Reinhart BJ, Slack FJ, Basson M, Pasquinelli AE, Bettinger JC, Rougvie AE, Horvitz HR, Ruvkun G (2000) The 21-nucleotide let-7 RNA regulates developmental timing in *Caenorhabditis elegans*. *Nature* 403: 901–906

Rybak A, Fuchs H, Smirnova L, Brandt C, Pohl EE, Nitsch R, Wulczyn FG (2008) A feedback loop comprising lin-28 and let-7 controls pre-let-7 maturation during neural stem-cell commitment. *Nat Cell Biol* 10: 987–993

Sanchez JG, Okreglicka K, Chandrasekaran V, Welker JM, Sundquist WI, Pornillos O (2014) The tripartite motif coiled-coil is an elongated antiparallel hairpin dimer. *Proc Natl Acad Sci USA* 111: 2494–2499

Schindler C, Shuai K, Prezioso VR, Darnell JE Jr (1992) Interferon-dependent tyrosine phosphorylation of a latent cytoplasmic transcription factor. *Science* 257: 809 – 813

Schulman BRM, Liang X, Stahlhut C, DelConte C, Stefani G, Slack FJ (2014) The let-7 microRNA target gene, Mlin41/Trim71 is required for mouse embryonic survival and neural tube closure. *Cell Cycle* 7: 3935 – 3942

Shu J, Wu C, Wu Y, Li Z, Shao S, Zhao W, Tang X, Yang H, Shen L, Zuo X *et al* (2013) Induction of pluripotency in mouse somatic cells with lineage specifiers. *Cell* 153: 963 – 975

Smith AG, Heath JK, Donaldson DD, Wong GG, Moreau J, Stahl M, Rogers D (1988) Inhibition of pluripotential embryonic stem cell differentiation by purified polypeptides. *Nature* 336: 688 – 690

Soto-Gutierrez A, Navarro-Alvarez N, Zhao D, Rivas-Carrillo JD, Lebkowski J, Tanaka N, Fox IJ, Kobayashi N (2007) Differentiation of mouse embryonic stem cells to hepatocyte-like cells by co-culture with human liver nonparenchymal cell lines. *Nat Protoc* 2: 347 – 356

Takahashi K, Yamanaka S (2006) Induction of pluripotent stem cells from mouse embryonic and adult fibroblast cultures by defined factors. *Cell* 126: 663 – 676

Tang J, Qu LK, Zhang J, Wang W, Michaelson JS, Degenhardt YY, El-Deiry WS, Yang X (2006) Critical role for Daxx in regulating Mdm2. *Nat Cell Biol* 8: 855 – 862

Teslaa T, Teitell MA (2015) Pluripotent stem cell energy metabolism: an update. *EMBO J* 34: 138 – 153

Torres-Fernandez LA, Jux B, Bille M, Port Y, Schneider K, Geyer M, Mayer G, Kolanus W (2019) The mRNA repressor TRIM71 cooperates with nonsense-mediated decay factors to destabilize the mRNA of CDKN1A/p21. *Nucleic Acids Res* 47: 11861 – 11879

Vander Heiden MG, Cantley LC, Thompson CB (2009) Understanding the Warburg effect: the metabolic requirements of cell proliferation. *Science* 324: 1029 – 1033

Wang Z, Oron E, Nelson B, Razis S, Ivanova N (2012) Distinct lineage specification roles for NANOG, OCT4, and SOX2 in human embryonic stem cells. *Cell Stem Cell* 10: 440 – 454

Webb BA, Forouhar F, Szu FE, Seetharaman J, Tong L, Barber DL (2015) Structures of human phosphofructokinase-1 and atomic basis of cancer-associated mutations. *Nature* 523: 111 – 114

Welte T, Tuck AC, Papasaikas P, Carl SH, Flemr M, Knuckles P, Rankova A, Buhler M, Grosshans H (2019) The RNA hairpin binder TRIM71 modulates alternative splicing by repressing MBNL1. *Genes Dev* 33: 1221 – 1235

Williams RL, Hilton DJ, Pease S, Willson TA, Stewart CL, Gearing DP, Wagner EF, Metcalf D, Nicola NA, Gough NM (1988) Myeloid leukaemia inhibitory factor maintains the developmental potential of embryonic stem cells. *Nature* 336: 684 – 687

Worringer KA, Rand TA, Hayashi Y, Sami S, Takahashi K, Tanabe K, Narita M, Srivastava D, Yamanaka S (2014) The let-7/LIN-41 pathway regulates reprogramming to human induced pluripotent stem cells by controlling expression of prodifferentiation genes. *Cell Stem Cell* 14: 40 – 52

Yang W, Xia Y, Hawke D, Li X, Liang J, Xing D, Aldape K, Hunter T, Alfred Yung WK, Lu Z (2012) PKM2 phosphorylates histone H3 and promotes gene transcription and tumorigenesis. *Cell* 150: 685 – 696

Ying Q-L, Nichols J, Chambers I, Smith A (2003) BMP induction of id proteins suppresses differentiation and sustains embryonic stem cell self-renewal in collaboration with STAT3. *Cell* 115: 281 – 292

Yu X, Li S (2017) Non-metabolic functions of glycolytic enzymes in tumorigenesis. *Oncogene* 36: 2629 – 2636

Yu L, Ji KY, Zhang J, Xu Y, Ying Y, Mai T, Xu S, Zhang QB, Yao KT, Xu Y (2019) Core pluripotency factors promote glycolysis of human embryonic stem cells by activating GLUT1 enhancer. *Protein Cell* 10: 668 – 680

Yuan F, Jin X, Li D, Song Y, Zhang N, Yang X, Wang L, Zhu WG, Tian C, Zhao Y (2019) ULK1 phosphorylates Mad1 to regulate spindle assembly checkpoint. *Nucleic Acids Res* 47: 8096 – 8110